ChemPhysMater 3 (2024) 204–211

Contents lists available at ScienceDirect

ChemPhysMater

journal homepage: https://www.keaipublishing.com/en/journals/chemphysmater/

Highly exposed Cu active sites as efficient peroxidase mimics for colorimetric analysis

Hengya Wei, Shushu Chu, Fangning Liu, Shengzhen Li, Yizhong Lu*

School of Materials Science and Engineering, University of Jinan, Jinan 250022, China

ARTICLE INFO

Keywords:
Nanozyme
Highly exposed active sites
Peroxidase-like
α-glucosidase
Sensing

ABSTRACT

Nanozymes are nanomaterials with intrinsic enzyme-mimic activity, but their large-scale application is generally limited by their low catalytic activity. Herein, we demonstrated that highly exposed Cu active sites on two-dimensional (2D) nitrogen-doped carbon (Cu_x/NC) can serve as efficient peroxidase-like (POD) catalysts with high atomic utilization. Specially, the uniformly distributed Cu active sites could react with H_2O_2 to produce singlet oxygen ($^1O_2$) under acidic conditions, which can efficiently oxidizes colorless 3,3′, 5,5′-tetramethylbenzidine (TMB) to blue oxidized TMB (oxTMB). Among various Cu_x/NC nanozymes studied, the $Cu_{0.14}$/NC exhibited smaller maximum catalytic velocities (V_{max}) and Menten constant (K_m) for TMB and H_2O_2. Benefiting from the highly active peroxidase-like activity, the $Cu_{0.14}$/NC nanozyme could be successfully applied for the hydroquinone (HQ) and ascorbic acid (AA) detection applications through the inhibitory effect of HQ and AA. More interestingly, α-glucosidase (α-Glu) detection sensing platform could be constructed based on HQ as a signal transmitter, with the detection range ranging from 0 to 12 U/L and the minimum detection limit being 0.68 U/L. This work provides not only an idea for the rational design of highly exposed Cu active sites but also fabricate an effective detection sensing platform for HQ, AA, and α-Glu detection.

1. Introduction

Peroxidases are thought to be essential oxidoreductase in organisms [1]. However, natural peroxidases usually have inherent some disadvantages, such as high cost and variability, which seriously hinder their practical application. In contrast, due to their excellent stability, low cost as well as high biocompatibility, nanozymes have been rapidly developed and widely used in biosensing, medical treatment, colorimetric detection, catalysis, antibacterial,and other fields [2]. At present, various nanomaterials (metal oxides [3–5], noble metals [6,7], non-noble metals [8,9], carbon-based materials [10,11]) have been developed as efficient peroxidase-like (POD) mimic enzymes. Nevertheless, traditional POD catalysts usually display some problems, such as poor biocompatibility, low activity, and selectivity. Therefore, novel nanozymes with improve enzyme-like activity and good stability are highly deserved.

To date, extensive studies have demonstrated that single-atom catalysts with atomically-precise structure and uniform distributed active sites could serve as potential nanozymes with high POD performance [12,13]. However, although some single-atom catalysts have been developed and used for peroxidase-mimics, only a small amount of metal content that exclusively located on the surface of them are utilized during the catalytic process. Thus, in order to maximum atom utilization efficiency of single-atom catalysts, metal active sites supported on two-dimensional nanosheets, where much more active sites may exposed extensively, could be expected and used as highly efficient peroxidase-mimics [14].

α-Glu is crucial in controlling glucose concentration and is an essential indicator of human health [15,16]. Therefore, it is necessary to design a reliable and sensitive detection method. Various detection methods including colorimetric detection [15,17,18], electrochemical detection [19], fluorescence detection [16,20,21] have been fabricated. Among them, colorimetric detection is most convenient. Moreover, total antioxidant capacity (TAC) is an important index to measure the antioxidant capacity of food. Establishing a highly selective and sensitive AA detection method is significant. According to the literature, both HQ and AA can inhibit the oxidation reaction of TMB, thus effectively inhibiting the activity of nanozymes [18,22]. The α-Glu will hydrolyze α-arbutin to produce HQ. Based on this, a colorimetric detection α-Glu sensing platform with HQ as a signal transmitter can be constructed.

In this work, highly exposed Cu active sites supported on 2D nitrogen doped-carbon nanosheets (Cu_x/NC) are developed and used for colorimetric analysis applications. The as-obtained $Cu_{0.14}$/NC nanozymes with excellent POD activity have been successfully applied to detect HQ and AA. On this basis, α-Glu detection sensing platform was constructed. In addition, we completed the determination of

* Corresponding author.
E-mail address: mse_luyz@ujn.edu.cn (Y. Lu).

https://doi.org/10.1016/j.chphma.2023.12.001
Received 23 October 2023; Received in revised form 21 November 2023; Accepted 6 December 2023
Available online 15 December 2023
2772-5715/© 2023 The Authors. Publishing Services by Elsevier B.V. on behalf of KeAi Communications Co. Ltd. This is an open access article under the CC BY license (http://creativecommons.org/licenses/by/4.0/)

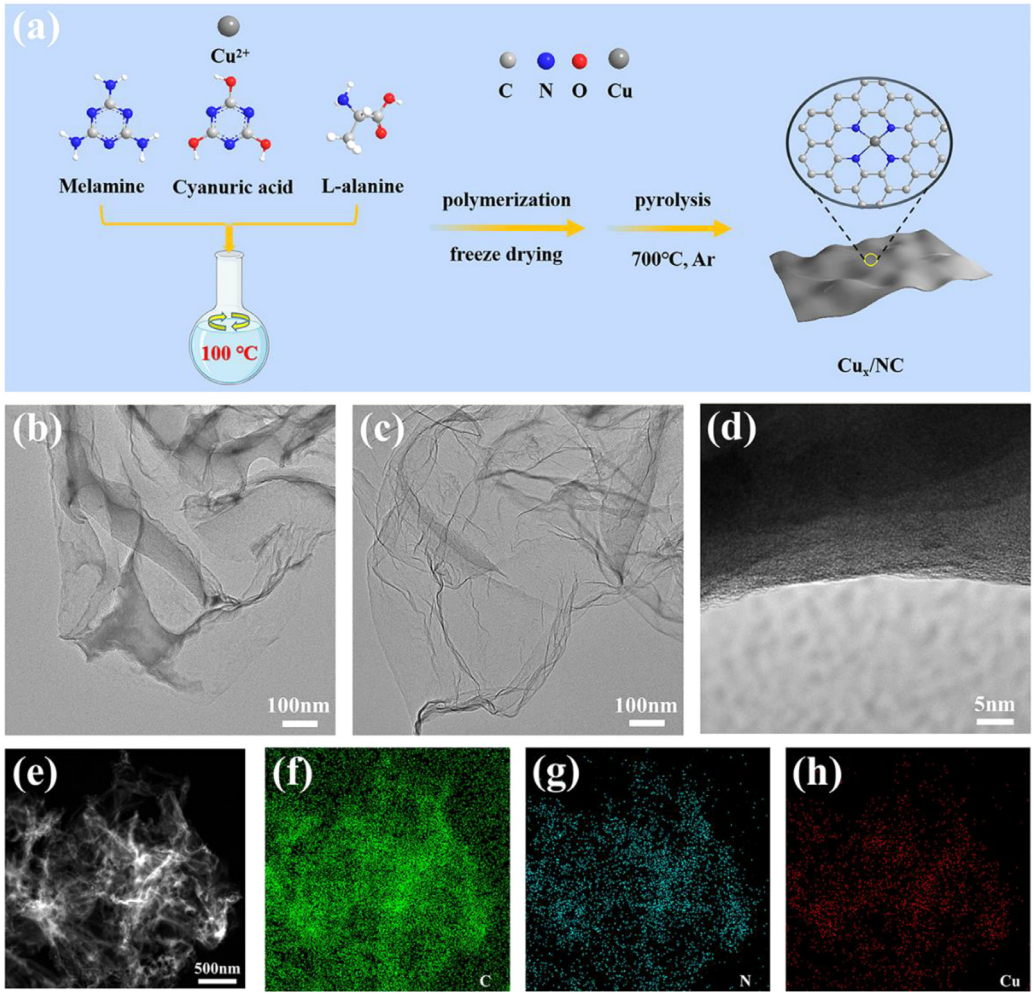

Fig. 1. (a) Cu_x/NC preparation diagram. TEM images of (b)(c) NC and $Cu_{0.14}$/NC. (d) HRTEM images of $Cu_{0.14}$/NC. (e)–(h) The corresponding EDS mapping of $Cu_{0.14}$/NC.

TAC content in actual samples, which further broadened its detection application.

2. Experimental section

2.1. Synthesis of Cu_x/NC

The synthesis procedure are strictly according to previous work [23]. Typically, 2 g of melamine, 2 g of cyanuric acid, and 2 g of L-alanine were dispersed in 100 mL of deionized water to form a homogeneous suspension by stirring at 100 °C. Then, 140 mg of $Cu(NO_3)_2{\cdot}3H_2O$ was slowly added to the above solution under stirring for 12 h at 100 °C, and the obtained slurry was then frozen in liquid nitrogen and freeze-dried. After freeze-drying, the collected powder was pyrolyzed under Ar atmosphere at 700 °C for 2 h. Finally, the obtained black powder was added to the H_2SO_4 (0.5 M) solution, stirred at 80 °C for 12 h, washed several times, and dried in a vacuum at 70 °C for 12 h. The synthetic process of NC, $Cu_{0.07}$/NC, and $Cu_{0.21}$/NC samples was the same with $Cu_{0.14}$/NC except that the precursor was added 0, 70, and 210 mg of $Cu(NO_3)_2{\cdot}3H_2O$, respectively.

2.2. POD activity of Cu_x/NC

To verify the POD activity of Cu_x/NC, TMB was used as the chromogenic substrate in the presence of H_2O_2. 890 μL of acetate buffer (0.2 M, pH = 4.0), 10 μL of Cu_x/NC solution (0.25 mg/mL), and 50 μL of H_2O_2 (10 mM) were thoroughly mixed, then 50 μL of TMB solution (5 mM) were added into the centrifugal tube and incubated at room temperature for 10 min. The absorbance of oxTMB was recorded.

3. Results and discussion

3.1. Synthesis and characterization of Cu_x/NC

Atomically-precise Cu nanozymes (Cu_x/NC) with typical Cu-N_4 structure were prepared by polycondensation and subsequent pyrolysis (Fig. 1(a)) [23]. Typically, melamine, cyanuric acid, and L-alanine was used as nitrogen source and carbon source, respectively. During the dissolution of melamine, cyanuric acid, L-alanine, and copper nitrate in aqueous solutions, Cu^{2+} is chelated in the polymer. Finally, the blue solid obtained after freeze-drying was pyrolyzed at 700 °C to form Cu-doped nitrogen-carbon nanostructures. For comparison, NC, $Cu_{0.07}$/NC and $Cu_{0.21}$/NC were alos obtained by simple adjusting the doping amount of Cu^{2+} ions. As shown in Figs. 1(b)(c) and S1(a)(c), the transmission electron microscopy (TEM) images reveal that all four samples are 2D nanosheets morphology, which indicates that the doping of Cu^{2+} ions does not change 2D nanosheets structure. High resolution TEM (HRTEM) images display that Cu_x/NC does not form Cu particles (Figs. 1(d) and S1(b)(d)). And the energy dispersive spectrometer (EDS) mappings (Figs. 1(e)–(h)) also show that Cu, C, and N are uniformly dis-

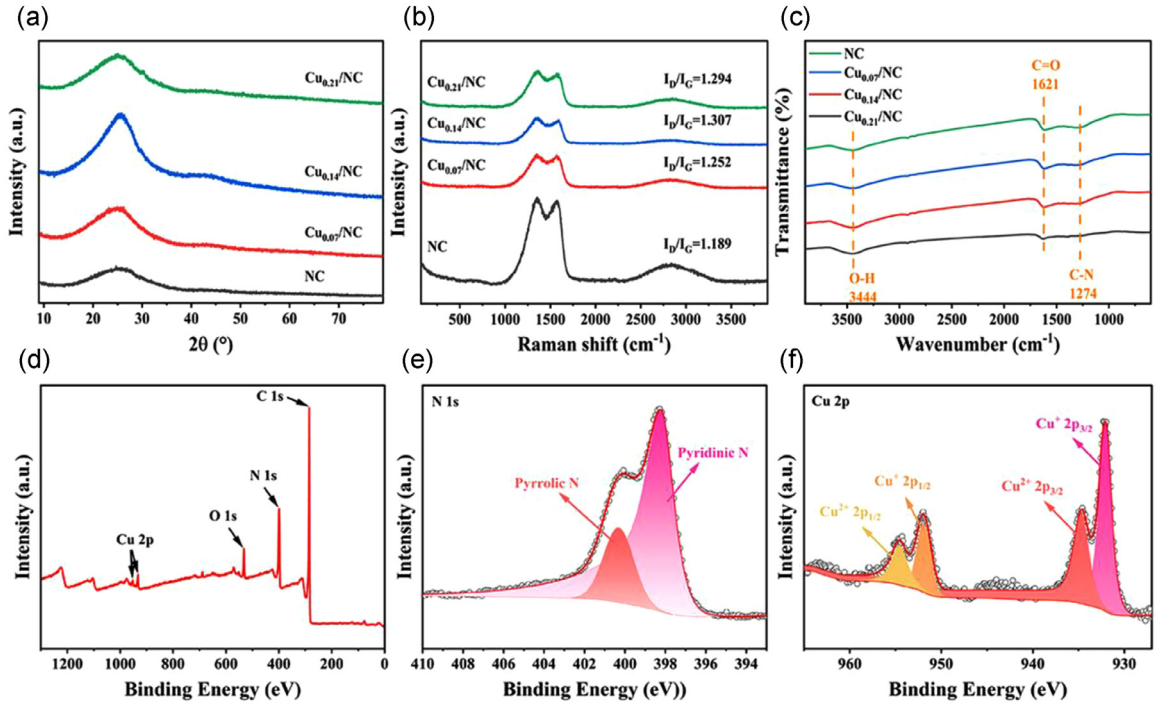

Fig. 2. (a)–(c) are XRD, Raman, and FTIR spectra of NC, $Cu_{0.07}$/NC, $Cu_{0.14}$/NC, and $Cu_{0.21}$/NC, respectively. (d) XPS spectra of $Cu_{0.14}$/NC. (e)(f) XPS spectra of N 1s and Cu 2p of $Cu_{0.14}$/NC.

persed in $Cu_{0.14}$/NC [24], indicating the Cu sites are isolated. All these results suggested the successful synthesis of Cu_x/NC catalysts.

As shown in Fig. 2(a), the X-ray diffraction (XRD) patterns of NC and Cu_x/NC display two typical peaks (25° and 44°) belonging to (002) and (100) crystal planes of graphite carbon [18], respectively. In addition, there are no other diffraction peaks, proving that there is no crystalline Cu species, further indicating that the Cu atoms are separately anchored on the carbon substrates. Raman spectroscopy also confirmed the formation of isolated Cu doping into the nitrogen-carbon structure (Fig. 2(b)). In the Raman spectra of NC and Cu_x/NC, Raman peaks are situated near 1350 and 1580 cm^{-1} in agreement with disordered carbon (D peak) and graphitic carbon (G peak), respectively [25]. The I_D/I_G values of NC, $Cu_{0.07}$/NC, $Cu_{0.14}$/NC, and $Cu_{0.21}$/NC were determined to be 1.189, 1.252, 1.307, and 1.294, respectively. The results show that the doping of Cu sites could not introduce more defects on carbon substrate and thus the improved activity due to the introduce of active Cu sites [18,26,27].

The chemical composition and bonding state of Cu_x/NC were studied by Fourier transform infrared spectroscopy (FTIR) and X-ray photoelectron spectroscopy (XPS). The FTIR analysis of Fig. 2(c) showed that the types of functional groups on the surface of nitrogen-doped carbon nanosheets do not change with the doping of Cu. The absorption peaks at 3444, 1621, and 1274 cm^{-1} are attributed to O–H, C=O, and C–N, respectively. The XPS spectra of Cu_x/NC in Figs. 2(d), S2(a), S3(a), and S4(a) proved that Cu, C, N, and O elements coexisted in the catalyst. As shown in Figs. 2(e), S2(b), S3(b), and S4(b), the high-resolution N 1s spectra show that 398.2 and 400.2 eV correspond to pyrrole nitrogen and pyridine nitrogen, respectively [28], which are the main N species in the catalyst. Notably, the higher pyridine nitrogen ratio in $Cu_{0.14}$/NC is conducive to promoting substrate and electron transport to enhance the catalytic ability of nanozymes [29]. The high-resolution spectra of Cu 2p shown in Figs. 2(f), S3(c), and S4(c) can be convoluted into four bands at 932.1, 934.6, 951.9, and 954.5 eV, corresponding to the binding energies of Cu^+ $2p_{3/2}$, Cu^{2+} $2p_{3/2}$, Cu^+ $2p_{1/2}$ and Cu^{2+} $2p_{1/2}$, respectively [30]. As known, Cu ions are reduced to metal Cu by carbon under high-temperature conditions. The high-resolution spectra of Cu 2p show that Cu exists in an isolated state in the catalyst and does not form metal particles, which means forming the Cu_x/NC structure.

3.2. POD activity of Cu_x/NC

2,2′-azinobis (3-ethylbenzothiazoline-6-sulfonic acid ammonium salt) (ABTS), o-phenylenediamine (OPD), and TMB were used as typical chromogenic substrates to evaluate the POD activity of Cu_x/NC preliminarily [31,32]. As shown in Figs. 3(a)–(c), in the presence of Cu_x/NC and H_2O_2, colorless ABTS, OPD, and TMB were oxidized, producing blue-green, yellow, and blue products with clear UV–visible spectral characteristic absorption peaks at 416, 448, and 652 nm. However, there is no apparent typical absorption peak signal in the case of only three substrates in the solution and no H_2O_2 involved in the reaction. These results confirm the intrinsic POD catalytic ability of the Cu_x/NC catalyst. As shown in Fig. 3(d), within 150 s of the reaction, with the increase of the amount of Cu contents, the POD activity increase firstly and then decrease. The POD activity of nanozymes is influenced by temperature and pH [24]. As shown in Fig. S5, the optimal pH of the reaction was determined to be 4.0, and the optimal reaction temperature was 55 °C.

3.3. Steady-state kinetic analysis and catalytic mechanism

The POD activity of NC and Cu_x/NC was evaluated by steady-state kinetic analysis. As shown in Figs. 4 and S6, the steady-state kinetic parameters of TMB and H_2O_2 were calculated, respectively. Compared with NC, $Cu_{0.07}$/NC, $Cu_{0.21}$/NC, and other nanozymes previously reported, $Cu_{0.14}$/NC has a smaller K_m and a larger V_{max} (Table S1). Therefore, it has a better affinity and faster reaction rate [32] for substrates (TMB and H_2O_2). The excellent association can promote its catalytic efficiency, and the quicker reaction rate can shorten the reaction time and ensure the timeliness of the subsequent colorimetric sensor. Due to the best POD activity of $Cu_{0.14}$/NC, it was applied in subsequent studies.

To gain a deeper insight into the catalytic mechanism of the reaction, various concentrations of l-tryptophan, isopropanol, and superoxide dismutase (SOD) were employed to effectively scavenge $^1O_2$, hydroxyl rad-

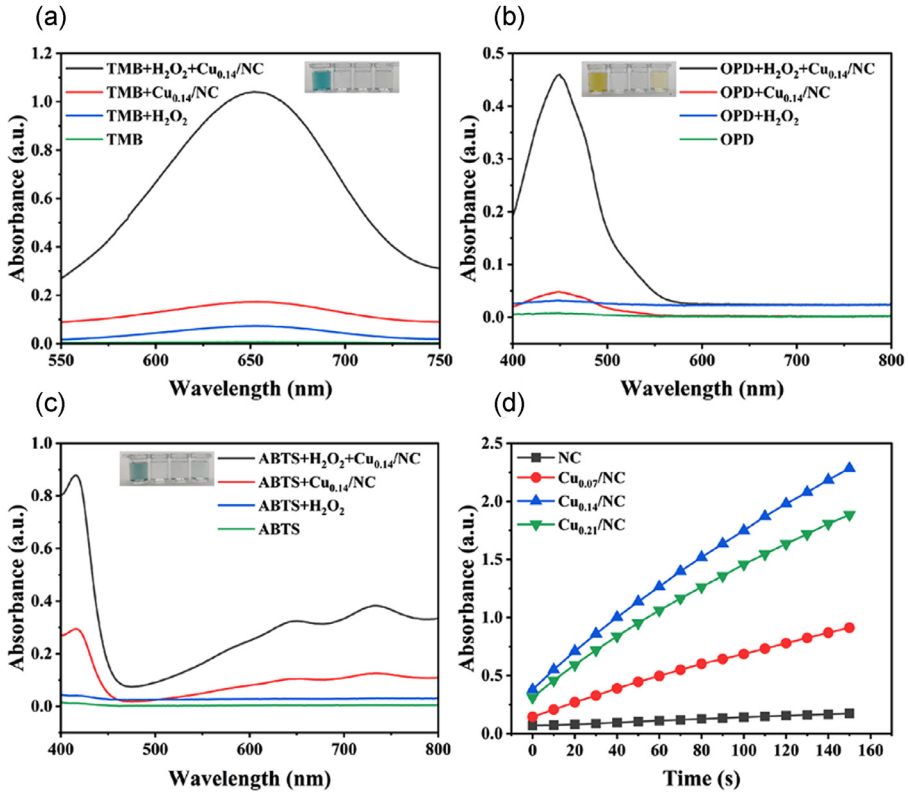

Fig. 3. (a)-(c) UV–vis absorption spectra of $Cu_{0.14}$/NC-H_2O_2 system with different substrates (TMB, OPD, and ABTS). (d) The relationship between absorbance and time of NC, $Cu_{0.07}$/NC, $Cu_{0.14}$/NC and $Cu_{0.21}$/NC.

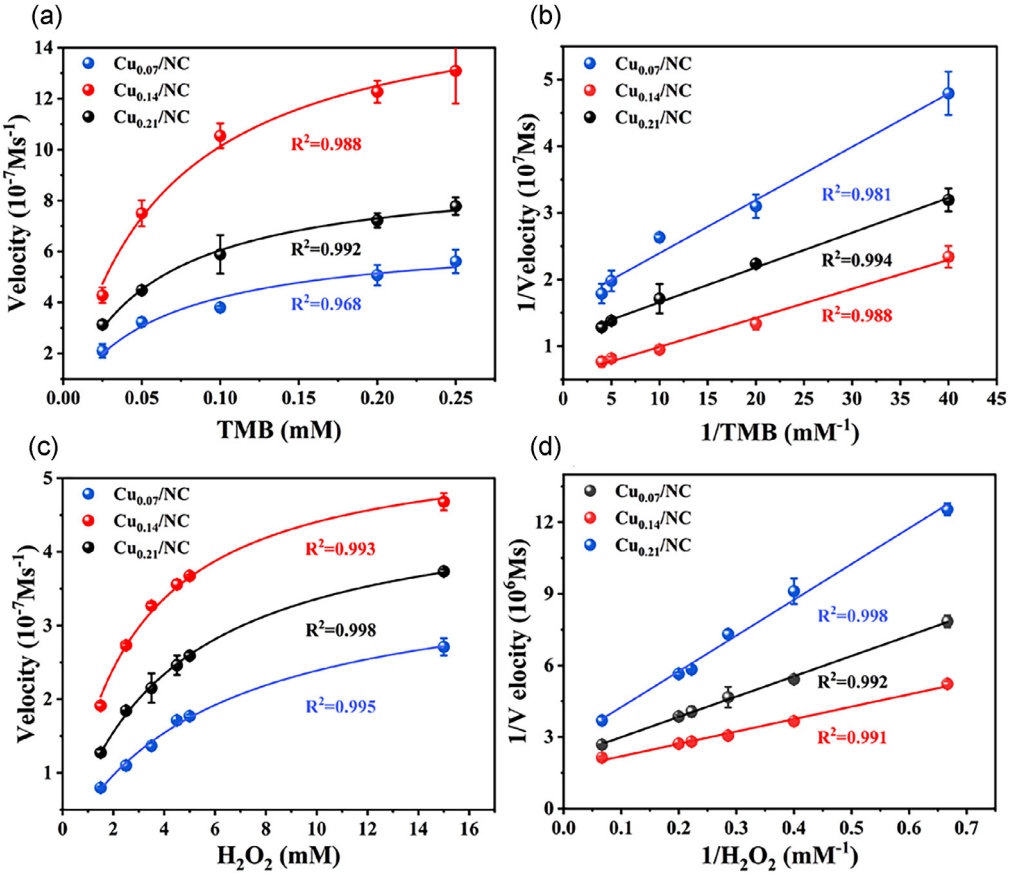

Fig. 4. Comparison of steady-state kinetics of $Cu_{0.07}$/NC, $Cu_{0.14}$/NC, and $Cu_{0.21}$/NC. Michaelis-Menten fitting curves of (a) TMB and (c) H_2O_2; Lineweaver-Burk plots of (b) TMB and (d) H_2O_2.

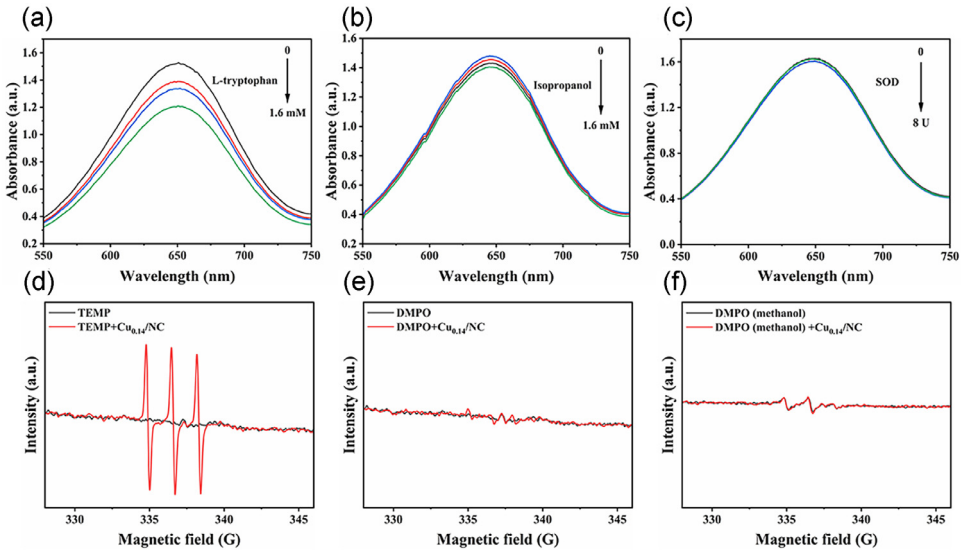

Fig. 5. (a)–(c) The change of solution habit after adding different concentrations of l-tryptophan, isopropanol and SOD. (d)–(f) ESR spectra measured under different conditions using TEMP and DMPO as capture agents.

ical (•OH), and superoxide free radicals ($•O_2^-$), aiming to investigate the reactive oxygen species [18,22,32,33]. As shown in Fig. 5(a), the absorbance of the system was significantly decreased after the addition of l-tryptophan. However, the absorbance of the system did not change significantly after isopropanol and SOD (Figs. 5(b)(c)), indicating that $^1O_2$ was the main active oxygen species, as further confirmed by electron spin resonance (ESR) spectroscopy (Figs. 5(d)–(f)). According to previous reports, the $^1O_2$ produced in the $Cu_{0.14}$/NC-H_2O_2-TMB system may be attributed to the coordination structure and distribution of Cu-NC, resulting in a unique Fenton-like reaction in the solution system [34,35]. In this process, H_2O_2 can generate $^1O_2$ through a two-step one-electron path under the catalysis of $Cu_{0.14}$/NC. In the first step, H_2O_2 generates $•OOH/•O_2^-$ under the catalysis of $Cu_{0.14}$/NC, and then $•OOH/•O_2^-$ is further oxidized to $^1O_2$ in the second step [35,36]. In addition, the catalytic active site of $Cu_{0.14}$/NC was analyzed by poisoning the catalytic site of metal center by SCN^- coordinating with Cu [37]. As depicted in Fig. S7, the absorbance of $Cu_{0.14}$/NC-H_2O_2-TMB system decreases with the increasing concentration of KSCN, indicating that Cu site was the main active site for $Cu_{0.14}$/NC nanozyme [38].

3.4. Detection of AA and HQ

According to previous reports, AA can be an antioxidant and free radical scavenger [39], based on this, we performed AA detection. As depicted in Fig. 6(a), the catalytic oxidation reaction proceeded normally in the $Cu_{0.14}$/NC-H_2O_2-TMB system solution (red line), and the absorbance at 652 nm instantly decreased after the introduction of AA. Moreover, the direct addition of AA to the system solution (blue line) inhibited the catalytic oxidation reaction, which was subsequently restored upon depletion of AA. The above results prove that the presence of AA can reduce oxTMB and eliminate $^1O_2$ produced, indicating the feasibility of $Cu_{0.14}$/NC to detect AA. With the increase of AA concentration from 0 to 250 μM, the absorbance of the $Cu_{0.14}$/NC-H_2O_2-TMB-AA system decreased (Figs. 6(b)(c)). In addition, AA showed an excellent linear relationship with the absorbance of TMB at 652 nm in the range of 0–200 μM, and the minimum detection limit was 0.33 μM. Compared with many previously reported works (Table S2), $Cu_{0.14}$/NC exhibits a wider linear range and higher sensitivity. When D(-)-fructose, d-glucose, sucrose, α-d-lactose monohydrate, D(+)-glucose, Cu^{2+}, K^+, Na^+, L-histidine, L-glutamic acid, L-valine, L-leucine, L-phenylalanine, L-serine and L-threonine were introduced into the system solution, the absorbance was almost unchanged (Fig. S8), proving the system had good selectivity.

Additionally, TAC can be used to evaluate antioxidant capacity in actual samples [40]. As shown in Fig. S9(a), fruits, beverages, and vitamin C tablets can effectively inhibit the color reaction of the $Cu_{0.14}$/NC-H_2O_2-TMB system. 5 kinds of fruits, 3 types of beverages, and 2 kinds of vitamin C tablets were selected for the TAC test, which proved the method's feasibility (Fig. S9(b)).

As a pollutant, HQ can cause irreversible damage to the human body [41,42]. With the process of industrialization, accurate detection of HQ content in the ecological environment is becoming more and more critical. As shown in Fig. 6(d), after HQ is added to the $Cu_{0.14}$/NC-H_2O_2-TMB system for 10 min, the absorbance of the system at 652 nm drops instantaneously and cannot be recovered within 10 min, which proved that HQ had strong reduction ability and free radical scavenging performance [18,43]. Fig. 6(e) depicted that the absorbance of the $Cu_{0.14}$/NC-H_2O_2-TMB-HQ system decreased, with the introduction of different concentrations of HQ in the range of 0–100 μM. Moreover, and in the field of 0–70 μM, the concentration of HQ showed an excellent linear relationship with the absorbance (Fig. 6(f)). The minimum detection limit was 0.34 μM (3 N/S), which is better than some previously reported methods (Table S3).

To verify the selectivity of the HQ detection sensing platform, hydroquinone, p-nitrophenol, resorcinol, phenol, o-nitrophenol, m-nitrophenol, and bisphenol A (BPA) were introduced into $Cu_{0.14}$/NC-H_2O_2-TMB-HQ system, respectively. Obviously, only when HQ is introduced the absorbance will decrease significantly, which proves that it has good selectivity and provides the possibility for later detection of HQ content in actual water samples (Fig. S10).

Furthermore, we have carried out standard recovery detection of HQ content in lake and tap water. As shown in Table 1, the recovery was in the range of 96.5%–105.8%, and the relative standard deviation (RSD) was between 1.35% and 5.46%. It is proved that the HQ sensing platform we designed has better development space in determining HQ content in the environment.

3.5. Detection of α-Glu

As we all know, as revealed in Fig. 7(a), α-Glu can catalyze the hydrolysis of α-arbutin to produce HQ to inhibit the peroxidase activity of $Cu_{0.14}$/NC [44,45]. As shown in Fig. 7(b), only when α-Glu and α-arbutin coexist in the system the absorbance of $Cu_{0.14}$/NC-H_2O_2-TMB

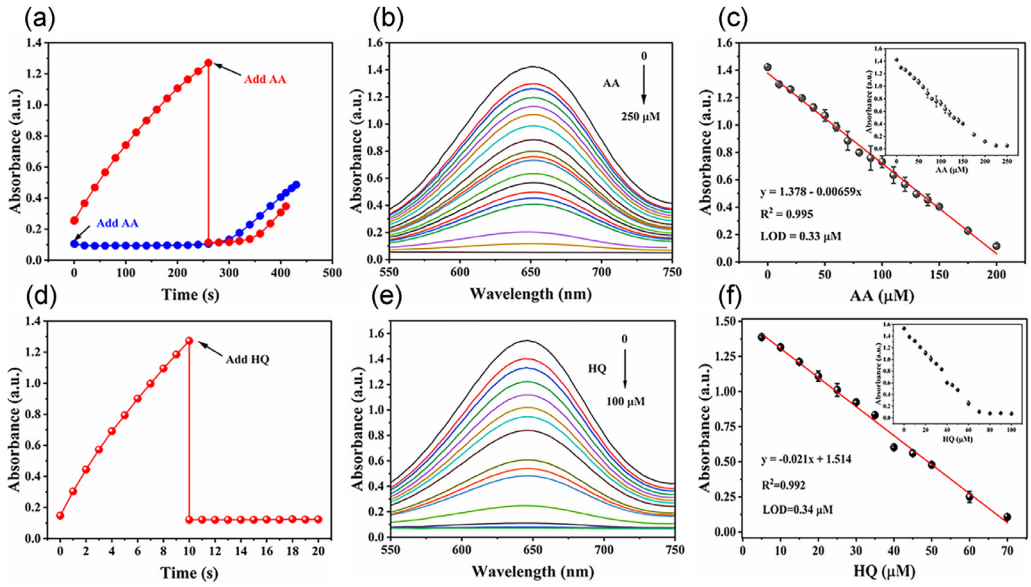

Fig. 6. (a)(d) The time-dependent absorbance at 652 nm of $Cu_{0.14}$/NC-catalyzed TMB oxidation and AA/HQ-mediated oxTMB reduction. (b)(e) The absorbance changes of the system solution after adding different concentrations of AA/HQ. (c)(f) The relationship between the concentration of AA/HQ and the absorbance at 652 nm.

Table 1
The content of HQ in lake water and tap water was detected by standard addition recovery.

Sample	Added (μM)	Found (μM)	Recover (%)	RSD (%, n = 3)
Sample 1	0	–	–	–
	15	15.9	105.8	1.60
	30	30.2	100.5	2.64
	45	43.4	96.5	1.81
Sample 2	0	–	–	–
	15	15.3	101.8	5.46
	30	29.3	97.8	1.35
	45	43.4	96.5	2.84

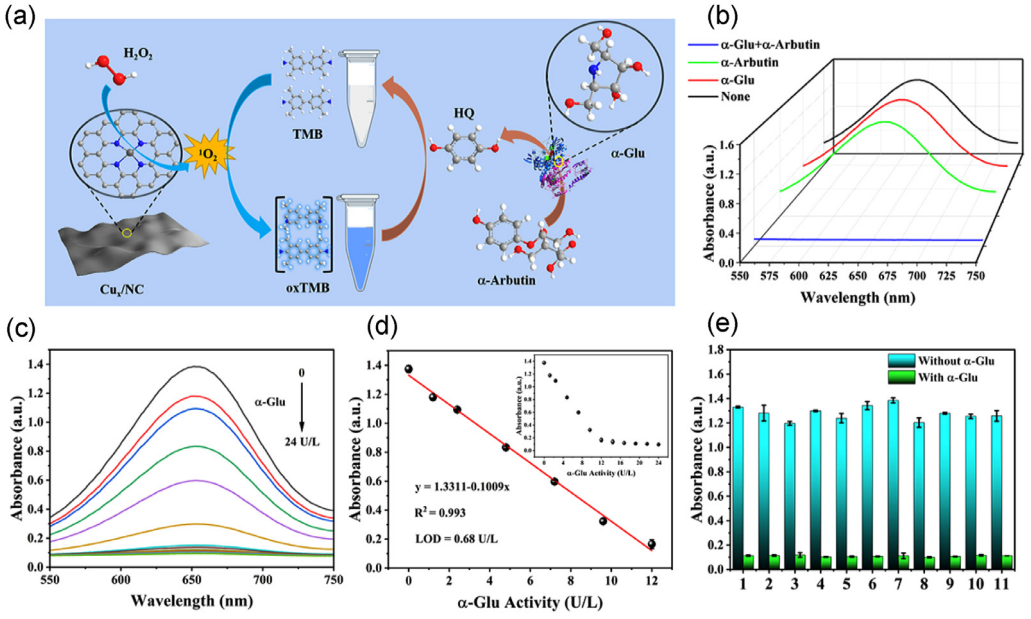

Fig. 7. (a) α-Glu activity detection diagram. (b) The UV–vis absorption spectra of different reaction systems. (c) The absorbance change of the system solution after adding another activity α-Glu. (d) The relationship between α-Glu activity and absorbance at 652 nm. (e) The absorbance was measured to detect control proteins/enzymes and inorganic ions in the absence and presence of α-Glu.

Table 2
Determination of α-glucosidase activity in human serum samples.

Sample	Added (U/L)	Found (U/L)	Recover (%)	RSD (%, n = 3)
Sample 1	0	–	–	–
	7.2	6.26	86.9	0.93
	9.6	10.04	104.7	1.59
	12.0	11.44	95.4	0.21
Sample 2	0	–	–	–
	7.2	6.82	94.6	3.27
	9.6	10.32	107.4	1.13
	12.0	11.34	94.4	0.79

system will be reduced, while α-Glu or α-arbutin alone will not affect the absorbance, which proves the feasibility of the α-Glu detection sensing platform. The incubation time and concentration of α-Glu and α-arbutin were optimized to enhance the sensitivity of the sensor platform. To facilitate the evaluation of the performance of the α-Glu detection sensing platform, design $\Delta A = A_0 - A$ (A: the absorbance at 652 nm is measured when there is α-Glu, A_0: the absorbance at 652 nm is measured when there is no α-Glu). As shown in Figs. S11(a)(b), with the increase of incubation time and α-arbutin concentration, ΔA gradually increased and tended to be stable. Here, the optimal incubation time was 50 min, and the optimal concentration of α-arbutin was 6 mM.

As shown in Figs. 7(c)(d), with the introduction of 0–24 U/L different activities of α-Glu, the concentration of HQ produced by the hydrolysis of α-arbutin catalyzed by α-Glu also increased, and the absorbance of the system at 652 nm gradually decreased. In the range of 0–12 U/L, the activity of α-Glu showed an excellent linear relationship with the absorbance, and the detection limit was 0.68 U/L (3 N/S), which is better than some previously reported methods (Table S4).

To verify anti-interference ability and selectivity in practical applications, L-lysine, L-valine, L-serine, L-threonine, glucose, fructose, lactose, Na^+, Mg^{2+}, and K^+ were selected to test the reliability of the platform. As shown in Fig. 7(e), the absorbance did not significantly change when these substances were added in the absence of α-Glu, indicating that only α-Glu could hydrolyze α-arbutin to produce HQ to inhibit the POD activity of $Cu_{0.14}$/NC, and the addition of these substances did not affect the detection of α-Glu in the presence of α-Glu. The above proves that the α-Glu detection sensing platform has excellent selectivity and anti-interference ability, which provides the possibility to detect the activity of α-Glu in vivo.

The validity and reliability of the method were evaluated by the determination of α-Glu in serum samples (Experimental design and procedures were approved by the Ethics Committee of University of Jinan (UJN-MSE-2023-002). Written informed consent was obtained from all participants). 7.2, 9.6, and 12 U/L of α-Glu were added to two human serum samples diluted 1000 times, and the samples were analyzed according to standard detection method. As listed in Table 2, the recovery rate was 86.9% to 107.4%, and the RSD was between 0.21%–3.27%, proving that the α-Glu detection sensing platform has good development prospects in practical biological detection applications.

4. Conclusions

In summary, highly exposed Cu active sites supported on 2D nitrogen-doped carbon nanosheets are designed and used as efficient peroxidase mimics. The as-obtained $Cu_{0.14}$/NC showed excellent POD activity with V_{max} of 1.806×10^{-7} Ms^{-1} for TMB and 5.966×10^{-7} Ms^{-1} for H_2O_2. The POD activity of $Cu_{0.14}$/NC is mainly due to the activation of H_2O_2 at the exposed Cu active sites to produce active $^1O_2$. Based on the inhibitory effect of AA and HQ on the POD activity, TAC and HQ detection sensing platform with high specificity were constructed. The detection results of actual samples show that the fabricated sensing platform could be used in practical applications. In addition, α-Glu detection sensing platform with high selectivity and anti-interference ability was created using α-Arbutin as the substrate and HQ as the signal transmitter. This work also provides some valuable references for designing and developing Cu-doped nanozymes to analyze small molecules.

Ethics approval

Experimental design and procedures were approved by the Ethics Committee of University of Jinan (UJN-MSE-2023-002). Written informed consent was obtained from all participants.

Declaration of Competing Interest

The authors declare that they have no known competing financial interests or personal relationships that could have appeared to influence the work reported in this paper.

CRediT authorship contribution statement

Hengya Wei: Investigation, Writing – original draft, Writing – review & editing. **Shushu Chu:** Investigation, Validation. **Fangning Liu:** Formal analysis, Data curation. **Shengzhen Li:** Supervision. **Yizhong Lu:** Conceptualization, Methodology, Resources.

Acknowledgements

This work was supported by the National Natural Science Foundation of China (22172063), the Young Taishan Scholar Program (tsqn201812080) and the Independent Cultivation Program of Innovation Team of Jinan City (2021GXRC052).

Supplementary materials

Supplementary material associated with this article can be found, in the online version, at doi:10.1016/j.chphma.2023.12.001.

References

[1] F. Liu, J. He, M. Zeng, J. Hao, Q. Guo, Y. Song, L. Wang, Cu–hemin metal-organic frameworks with peroxidase-like activity as peroxidase mimics for colorimetric sensing of glucose, J. Nanopart. Res. 18 (2016) 106.
[2] X. Cai, L. Jiao, H. Yan, Y. Wu, W. Gu, D. Du, Y. Lin, C. Zhu, Nanozyme-involved biomimetic cascade catalysis for biomedical applications, Mater. Today 44 (2021) 211–228.
[3] J. Feng, P. Huang, S. Shi, K.Y. Deng, F.Y. Wu, Colorimetric detection of glutathione in cells based on peroxidase-like activity of gold nanoclusters: A promising powerful tool for identifying cancer cells, Anal. Chim. Acta 967 (2017) 64–69.
[4] Y. Wang, Y. Liu, F. Ding, X. Zhu, L. Yang, P. Zou, H. Rao, Q. Zhao, X. Wang, Colorimetric determination of glutathione in human serum and cell lines by exploiting the peroxidase-like activity of CuS-polydopamine-Au composite, Anal. Bioanal. Chem 410 (2018) 4805–4813.
[5] T. Rohani Bastami, Z. Dabirifar, AuNPs@PMo_{12} nanozyme: Highly oxidase mimetic activity for sensitive and specific colorimetric detection of acetaminophen, RSC Adv. 10 (2020) 35949–35956.
[6] X. Wang, L. Qin, M. Zhou, Z. Lou, H. Wei, Nanozyme sensor arrays for detecting versatile analytes from small molecules to proteins and cells, Anal. Chem. 90 (2018) 11696–11702.
[7] X. Jiang, X. Wang, A. Lin, H. Wei, In situ exsolution of noble-metal nanoparticles on perovskites as enhanced peroxidase mimics for bioanalysis, Anal. Chem. 93 (2021) 5954–5962.

[8] Y.Z. Li, T.T. Li, W. Chen, Y.Y. Song, Co_4N nanowires: Noble-metal-free peroxidase mimetic with excellent salt- and temperature-resistant abilities, ACS Appl. Mater. Interfaces 9 (2017) 29881–29888.
[9] P. Singh, R.P. Ojha, S. Kumar, A.K. Singh, R. Prakash, Fe-doped MoS_2 nanomaterials with amplified peroxidase mimetic activity for the colorimetric detection of glutathione in human serum, Mater. Chem. Phys. 267 (2021) 124684.
[10] F. Qu, T. Li, M. Yang, Colorimetric platform for visual detection of cancer biomarker based on intrinsic peroxidase activity of graphene oxide, Biosens. Bioelectron. 26 (2011) 3927–3931.
[11] R. Li, M. Zhen, M. Guan, D. Chen, G. Zhang, J. Ge, P. Gong, C. Wang, C. Shu, A novel glucose colorimetric sensor based on intrinsic peroxidase-like activity of C60-carboxyfullerenes, Biosens. Bioelectron. 47 (2013) 502–507.
[12] D. Lin, S. Wu, S. Chu, Y. Lu, Cobalt-nitrogen co-doped carbon as highly efficient oxidase mimics for colorimetric assay of nitrite, Biosensors (2023).
[13] S. Xu, S. Zhang, Y. Li, J. Liu, Facile synthesis of iron and nitrogen co-doped carbon dot nanozyme as highly efficient peroxidase mimics for visualized detection of metabolites, Molecules (2023).
[14] B. Yuan, H.L. Chou, Y.K. Peng, Disclosing the origin of transition metal oxides as peroxidase (and catalase) mimetics, ACS Appl. Mater. Interfaces 14 (2022) 22728–22736.
[15] S. Nsanzamahoro, W.F. Wang, Y. Zhang, C.B. Wang, Y.P. Shi, J.L. Yang, α-glucosidase-triggered reaction for fluorometric and colorimetric assays based on the formation of silicon-containing nanoparticles, Anal. Chem. 93 (2021) 15412–15419.
[16] J. Zhang, J. Liu, M. Wang, G. Wang, X. Su, A fluorometric assay for α-glucosidase activity based on quaternary AgInZnS QDs, Microchim. Acta 188 (2021) 227.
[17] J. Zhang, Y. Liu, J. Lv, G. Li, A colorimetric method for α-glucosidase activity assay and its inhibitor screening based on aggregation of gold nanoparticles induced by specific recognition between phenylenediboronic acid and 4-aminophenyl-α-D-glucopyranoside, Nano Res. 8 (2015) 920–930.
[18] G. Kang, W. Liu, F. Liu, Z. Li, X. Dong, C. Chen, Y. Lu, Single-atom Pt catalysts as oxidase mimic for p-benzoquinone and α-glucosidase activity detection, Chem. Eng. J. 449 (2022) 137855.
[19] J. Li, G. He, B. Wang, L. Shi, T. Gao, G. Li, Fabrication of reusable electrochemical biosensor and its application for the assay of α-glucosidase activity, Anal. Chim. Acta 1026 (2018) 140–146.
[20] J. Liu, X. Duan, M. Wang, X. Su, A label-free fluorescent sensor based on silicon quantum dots–MnO_2 nanosheets for the detection of α-glucosidase and its inhibitor, Analyst 144 (2019) 7398–7405.
[21] H. Zhang, Z. Wang, X. Yang, Z.L. Li, L. Sun, J. Ma, H. Jiang, The determination of α-glucosidase activity through a nano fluorescent sensor of F-PDA−CoOOH, Anal. Chim. Acta 1080 (2019) 170–177.
[22] W. Liu, L. Chu, C. Zhang, P. Ni, Y. Jiang, B. Wang, Y. Lu, C. Chen, Hemin-assisted synthesis of peroxidase-like Fe-N-C nanozymes for detection of ascorbic acid-generating bio-enzymes, Chem. Eng. J. 415 (2021) 128876.
[23] H. Jin, P. Cui, C. Cao, X. Yu, R. Zhao, D. Ma, W. Song, Understanding the density-dependent activity of Cu single-atom catalyst in the benzene hydroxylation reaction, ACS Catal. 13 (2023) 1316–1325.
[24] J. Hao, C. Zhang, C. Feng, Q. Wang, Z.Y. Liu, Y. Li, J. Mu, E.C. Yang, Y. Wang, An ultra-highly active nanozyme of Fe,N co-doped ultrathin hollow carbon framework for antibacterial application, Chin. Chem. Lett. 34 (2023) 107650.
[25] X. Luo, J. Huang, J. Li, L. Cao, Y. Cheng, L. Guo, Y. Wang, H. Qi, Sn-C bonding anchored SnSe nanoparticles grown on carbon nanotubes for high-performance lithium-ion battery anodes, Appl. Surf. Sci. 491 (2019) 95–104.
[26] Z. Lin, H. Huang, L. Cheng, Y. Yang, R. Zhang, Q. Chen, Atomically dispersed Mn within carbon frameworks as high-performance oxygen reduction electrocatalysts for zinc–air battery, ACS Sustain. Chem. Eng. 8 (2020) 427–434.
[27] Z. Mu, S. Wu, J. Guo, M. Zhao, Y. Wang, Dual mechanism enhanced peroxidase-like activity of iron–nickel bimetal–organic framework nanozyme and its application for biosensing, ACS Sustain. Chem. Eng. 10 (2022) 2984–2993.
[28] K. Chen, R. Huang, F. Gu, Y. Du, Y. Song, A novel hollow Co_3O_4@N-doped carbon nanobubble film composite for high-performance anode of lithium-ion batteries, Compos. Part B: Engineer. 224 (2021) 109247.
[29] Y. Shang, Y. Ding, P. Zhang, M. Wang, Y. Jia, Y. Xu, Y. Li, K. Fan, L. Sun, Pyrrolic N or pyridinic N: The active center of N-doped carbon for CO_2 reduction, Chin. J. Catal. 43 (2022) 2405–2413.
[30] X. Liu, F. Wu, X. Zheng, H. Liu, F. Ren, J. Sun, H. Ding, R. Yang, L. Jin, Facile synthesis of high-loading Cu single-atom nanozyme for total antioxidant capacity sensing, ACS Appl. Nano Mater. 6 (2023) 10303–10311.
[31] C. Xia, X. Zhang, X. Liu, D. Wu, L. Guo, Old dogs, new trick: Classical starch-sodium iodide reagent as the chromogenic substrate of peroxidase-like nanozymes, Sens. Actuators B 368 (2022) 132229.
[32] H. Sun, W. Guo, Y. Han, Z. Gou, Y. Liang, J. Dan, Y. Kang, J. Wang, W. Zhang, Food-borne melanoidin based peroxidase mimic for the precise detection of total antioxidant capacity, Microchem. J. 184 (2023) 108161.
[33] Z. Li, F. Liu, S. Zhu, Z. Liu, F. Zhang, P. Ni, C. Chen, Y. Jiang, Y. Lu, Carbon nanotubes regulated by oxidizing functional groups as peroxidase mimics for total antioxidant capacity determination, Biosens. Bioelectr.: X 11 (2022) 100190.
[34] S. Zuo, Z. Guan, F. Yang, D. Xia, D. Li, Reactive oxygen species regulation and synergistic effect for effective water purification through Fenton-like catalysis on single-atom Cu–N sites, J. Mater. Chem. A 10 (2022) 10503–10513.
[35] F. Xu, C. Lai, M. Zhang, B. Li, L. Li, S. Liu, D. Ma, X. Zhou, H. Yan, X. Huo, B. Wang, H. Yi, L. Qin, L. Tang, High-loaded single-atom Cu-N_3 sites catalyze hydrogen peroxide decomposition to selectively induce singlet oxygen production for wastewater purification, Appl. Catal. B 339 (2023) 123075.
[36] Z. Yang, J. Qian, A. Yu, B. Pan, Singlet oxygen mediated iron-based Fenton-like catalysis under nanoconfinement, Proc. Natl. Acad. Sci. 116 (2019) 6659–6664.
[37] H.-W. Liang, S. Brüller, R. Dong, J. Zhang, X. Feng, K. Müllen, Molecular metal–Nx centres in porous carbon for electrocatalytic hydrogen evolution, Nat. Commun. 6 (2015) 7992.
[38] X. Zhou, L.-J. Wan, Y.-G. Guo, Synthesis of MoS_2 nanosheet–graphene nanosheet hybrid materials for stable lithium storage, Chem. Commun. 49 (2013) 1838–1840.
[39] Y. Jiang, N. Song, C. Wang, N. Pinna, X. Lu, A facile synthesis of Fe_3O_4/nitrogen-doped carbon hybrid nanofibers as a robust peroxidase-like catalyst for the sensitive colorimetric detection of ascorbic acid, J. Mater. Chem. B 5 (2017) 5499–5505.
[40] Z. Lou, S. Zhao, Q. Wang, H. Wei, N-Doped carbon as peroxidase-like nanozymes for total antioxidant capacity assay, Anal. Chem. 91 (2019) 15267–15274.
[41] E. Han, Y. Yang, Z. He, J. Cai, X. Zhang, X. Dong, Development of tyrosinase biosensor based on quantum dots/chitosan nanocomposite for detection of phenolic compounds, Anal. Biochem. 486 (2015) 102–106.
[42] C. Lou, T. Jing, J. Zhou, J. Tian, Y. Zheng, C. Wang, Z. Zhao, J. Lin, H. Liu, C. Zhao, Z. Guo, Laccase immobilized polyaniline/magnetic graphene composite electrode for detecting hydroquinone, Int. J. Biol. Macromol. 149 (2020) 1130–1138.
[43] X. Zheng, Z. Liu, Q. Lian, H. Liu, L. Chen, L. Zhou, Y. Jiang, J. Gao, Preparation of flower-like $NiMnO_3$ as oxidase mimetics for colorimetric detection of hydroquinone, ACS Sustain. Chem. Eng. 9 (2021) 12766–12778.
[44] G. Liu, J. Zhao, M. Yan, S. Zhu, W. Dou, J. Sun, X. Yang, In situ formation of fluorescent silicon-containing polymer dots for alkaline phosphatase activity detection and immunoassay, Sci. China Chem. 63 (2020) 554–560.
[45] M. Bekhit, T. Blazek, W. Gorski, Electroanalysis of enzyme activity in small biological samples: alkaline phosphatase, Anal. Chem. 93 (2021) 14280–14286.